Phonon Trigonal Warping Effect in Graphite and Carbon Nanotubes

Ge. G. Samsonidze,[1] R. Saito,[4,5] A. Jorio,[6,2] A. G. Souza Filho,[7,2] A. Grüneis,[4] M. A. Pimenta,[6] G. Dresselhaus,[3] and M. S. Dresselhaus[1,2]

[1]*Department of Electrical Engineering and Computer Science, Massachusetts Institute of Technology, Cambridge, Massachusetts 02139-4307*

[2]*Department of Physics, Massachusetts Institute of Technology, Cambridge, Massachusetts 02139-4307*

[3]*Francis Bitter Magnet Laboratory, Massachusetts Institute of Technology, Cambridge, Massachusetts 02139-4307*

[4]*Department of Electronic Engineering, University of Electro-Communications, Tokyo, 182-8585, Japan*

[5]*CREST JST, Tokyo, 182-8585, Japan*

[6]*Departamento de Física, Universidade Federal de Minas Gerais, Belo Horizonte, MG 30123-970, Brazil*

[7]*Departamento de Física, Universidade Federal do Ceará, Fortaleza, CE 60455-760, Brazil*

(Received 14 August 2002; published 15 January 2003)

The one-dimensional structure of carbon nanotubes leads to quantum confinement of the wave vectors for the electronic states, thus making the double resonance Raman process selective, not only of the *magnitude*, but also of the *direction* of the phonon wave vectors. This additional selectivity allows us to reconstruct the phonon dispersion relations of 2D graphite, by probing individual single wall carbon nanotubes of different chiralities by resonance Raman spectroscopy, and using different laser excitation energies. In particular, we are able to measure the *anisotropy*, or the trigonal warping effect, in the *phonon dispersion* relations around the hexagonal corner of the Brillouin zone of graphite.

DOI: 10.1103/PhysRevLett.90.027403 PACS numbers: 78.30.Na, 63.22.+m, 78.66.Tr, 81.05.Tp

Resonance Raman spectroscopy (RRS) has been shown to provide a valuable tool for probing the phonon dispersion relations of graphite $\omega_{\mathrm{ph}}(\mathbf{q})$ [1], which is complementary to inelastic neutron scattering, the phonon probe that is most commonly used today [2]. This is achieved by utilizing the double resonance (DR) mechanism [3], which couples electronic and phonon wave vectors. RRS in graphitic materials provides information on $\omega_{\mathrm{ph}}(\mathbf{q})$ around high symmetry points in the 2D hexagonal Brillouin zone (BZ) of the graphene layer (hexagonal corner at K, and center at Γ). However, use of the DR process as a phonon probe, as previously discussed [1], exhibits a significant limitation by averaging experimental data over the various directions of the phonon wave vector. This limitation can be overcome in low-dimensional systems, such as single wall carbon nanotubes (SWNTs), when the quantum confinement of the electronic and phonon states helps to separate wave vectors of different directions in the DR process. For RRS on isolated SWNTs, the magnitude of the resonant electronic and phonon wave vectors is determined by the laser excitation energy, according to regular DR theory [1], while the direction of the wave vectors is related to the SWNT chiral angle θ. In particular, the amount of anisotropy of $\omega_{\mathrm{ph}}(\mathbf{q})$ around the K and Γ points in the 2D BZ of graphite can be measured by RRS on isolated SWNTs of various chiralities.

A four-neighbor force-constant model [4] is commonly used to describe $\omega_{\mathrm{ph}}(\mathbf{q})$ of graphite and, consequently, of SWNTs with the help of the zone-folding scheme [4]. The force constants that have been fitted to inelastic neutron scattering data [2] and those fitted to DR Raman scattering data [5] show different amounts of anisotropy in $\omega_{\mathrm{ph}}(\mathbf{q})$ about the K and Γ points in the 2D BZ. In what follows, we consider quantitatively the amount of anisotropy for the Raman-active phonon mode near the K point responsible for the D- and G'-band Raman features of graphite. Since the G'-band is the strongest double resonance feature in the Raman spectra of individual SWNTs, it provides the most accurate experimental data on the anisotropy in $\omega_{\mathrm{ph}}(\mathbf{q})$. For quantitative characterization of the anisotropy, the difference in the phonon frequencies $\Delta\omega_{\mathrm{ph}}$ along two opposite directions KM and $K\Gamma$ in the 2D BZ at a special distance q_0 from the K point is introduced. Averaging the phonon wave vectors along different directions resonant with the Ar^+ laser line 2.41 eV gives $q_0 = 0.24K\Gamma$. It happens accidentally that q_0 is very close to $1/a$, where $a = \sqrt{3}a_{C-C}$, and $a_{C-C} =$ 1.42 Å is the interatomic distance in graphite and in SWNTs. For the Raman-active phonon mode near the K point, $\Delta\omega_{\mathrm{ph}} = -7\ \mathrm{cm}^{-1}$ was calculated using force constants fitted to neutron scattering data [2], and $\Delta\omega_{\mathrm{ph}} =$ $1\ \mathrm{cm}^{-1}$ for those fitted to DR Raman scattering data [5]. The first number is not reliable, since neutron scattering is not accurate near the K point, while the second number shows essentially no anisotropy, because DR Raman scattering, as previously applied, averages out different directions around the K point for measurements on highly oriented pyrolytic graphite (HOPG), graphite whiskers, and SWNT bundles, which were all used to fit the force constants [5]. In the present Letter, we show that $\Delta\omega_{\mathrm{ph}}$ can be measured accurately at the single nanotube level, yielding $\Delta\omega_{\mathrm{ph}} = 24\ \mathrm{cm}^{-1}$.

RRS in the graphite basal plane involves all the electronic states with wave vectors along the equienergy contour corresponding to a given laser excitation energy.

The three equienergy contours corresponding to the three E_{laser} values 1.58, 2.41, and 2.54 eV commonly used in RRS studies are plotted in Fig. 1(a), where k space in the vicinity of the K point in the 2D BZ of graphite is shown. Compared to the case of graphite, the number of electronic states in SWNTs is limited by quantum confinement to a subset of *allowed states*, and these can be picked out by the zone-folding scheme [4]. For each SWNT, the allowed states are given by parallel equidistant lines in the 2D BZ called "cutting lines." The distance between adjacent cutting lines $|\mathbf{K}_1| = 2/d_t$ is inversely proportional to the SWNT diameter d_t, while the orientation of the cutting lines is given by the SWNT chiral angle θ between them and the line connecting the nearest M points in the 2D BZ [4]. Four cutting lines are shown in Fig. 1(a) by grey lines on either side of the K point, two for zigzag ($\theta = 0$) and two for armchair ($\theta = \pi/6$) SWNTs. The Van Hove singularities (VHSs) in the density of states (DOS) of SWNTs appear at points k_i in the 2D BZ where the cutting lines are tangential to the equienergy contours. When the SWNT chirality changes from $\theta = 0$ to $\pi/6$, the two k_i vectors at the VHSs on either side of the K point move along the equienergy contour, taking all possible directions away from the K point, such as $K\Gamma$ and KM for zigzag SWNTs, and two equivalent directions between $K\Gamma$ and KM for armchair SWNTs [see Fig. 1(a)].

For the DR processes in graphite (for intervalley transitions between the K and K' points in the 2D BZ), the momentum conservation for the electron-phonon interaction couples the phonon q and electronic k wave vectors (measured from the nearest K or K' point in the 2D BZ) by the approximate relation $q \simeq 2k$ [6], or, in vector form, $\mathbf{q} \simeq -2\mathbf{k}$, where the "$-$" sign reflects the fact that the k vector along the $K\Gamma$ direction corresponds to the q vector along KM, and vice versa. In the case of 1D SWNTs, momentum conservation for the electron-phonon interaction requires both 1D wave vector conservation along the SWNT axis (along the $\mathbf{K}_2$ vector [4] in the 2D BZ) and wave function matching in the circumferential direction (along the $\mathbf{K}_1$ vector [4] in the 2D BZ). To account for both the 1D wave vector conservation and the wave function matching within the zone-folding scheme, the 1D BZ of the SWNT is unfolded into the 2D BZ of graphite, and the 2D wave vector conservation in the 2D BZ is considered, leading to the relation $\mathbf{q} = -2\mathbf{k}$, similar to the case of graphite. Here, $\mathbf{q}$ and $\mathbf{k}$ are not the 1D wave vectors in the 1D BZ of the SWNT, but rather are the 2D wave vectors in the unfolded 2D BZ of graphite. The relation becomes exact for SWNTs compared to graphite because of the quantum confinement of $\mathbf{q}$ and $\mathbf{k}$ in SWNTs. At the VHS E_{ii}, the relation turns into $\mathbf{q}_i = -2\mathbf{k}_i$. By $\mathbf{k}_i$ we refer to the initial electronic state in the valence band $\mathbf{k}_i^v$ but not to the optically excited electronic state in the conduction band $\mathbf{k}_j^c$. The optical transition is vertical in the unfolded 2D BZ ($\mathbf{k}_j^c = \mathbf{k}_i^v$) only for light polarization parallel to the SWNT axis (Z), while, for the perpendicular polarization (X), the electron is brought to the adjacent cutting line ($\mathbf{k}_j^c = \mathbf{k}_i^v \pm \mathbf{K}_1$) [7]. Thus, depending on the incident and scattered light polarizations, the double resonance condition changes, $\mathbf{q}_i = -2\mathbf{k}_i^v + \mu\mathbf{K}_1$, where $\mu = 0$ for ZZ, $\mu = 0, \pm 1, \pm 2$ for ZX and XZ, and $\mu = 0, \pm 2$ for XX polarizations of the incident/scattered light. A similar relation for the single resonance Raman process (the G band) $\mathbf{q}_i = \mu\mathbf{K}_1$ results in the appearance of Raman-active phonon modes of A, E_1, and E_2 symmetries for $\mu = 0$, $\mu = \pm 1$, and $\mu = \pm 2$, respectively [8]. We here consider only the case of ZZ polarization, since the X polarizations are considerably suppressed by the depolarization effect [9]. Thus, the DR condition for SWNTs is given by $\mathbf{q}_i = -2\mathbf{k}_i$, and both $\mathbf{q}_i$ and $\mathbf{k}_i$ take all possible directions between $K\Gamma$ and KM when the SWNT chirality changes from $\theta = 0$ (zigzag) to $\theta = \pi/6$ (armchair). The selection rules for intravalley transitions within the same K point in the 2D BZ can be considered in a similar way.

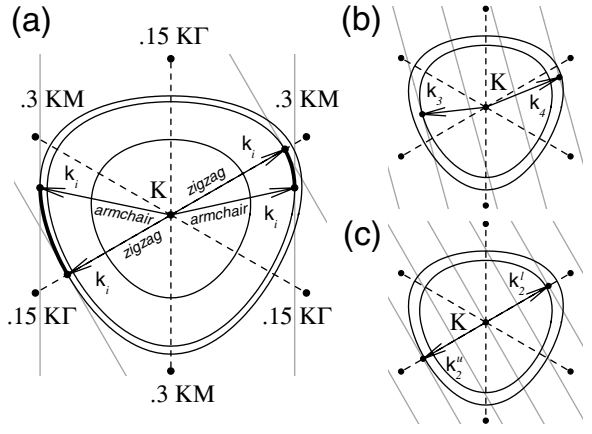

FIG. 1. (a) The electronic wave vectors k_i of the VHSs in SWNTs of zigzag and armchair structural symmetries. Three equienergy contours are shown for laser energies 1.58, 2.41, and 2.54 eV. Cutting lines for (b) semiconducting (17,6) and (c) metallic (27,0) SWNTs. Two equienergy contours in (b) and (c) are shown for resonance with the incident $E_{\text{laser}} = 2.41$ eV and G'-band scattered 2.08 eV light. Indices l and u in (c) denote lower and upper energy components of the VHS E_{22}^{M}.

RRS in SWNTs is enhanced when E_{laser} matches the transition energy E_{ii} between two VHSs in the valence (k_i^v) and conduction (k_i^c) bands at wave vector k_i in the 2D BZ for the case of ZZ polarization. This enhancement is sufficiently large to allow observation of RRS from individual SWNTs [10]. The distinctive structure of the VHSs in the DOS of each (n, m) SWNT [4] plays a key role in determining the (n, m) indices of SWNTs by RRS at the single nanotube level [10]. These distinctive VHSs for each (n, m) SWNT arise from anisotropy in the electronic dispersion relations $E(k)$ about the K point, which is known as the electronic trigonal warping effect [11]. In a similar fashion, anisotropy in $\omega_{\text{ph}}(\mathbf{q})$ is called the

phonon trigonal warping effect. The phonon trigonal warping effect explicitly affects the Raman spectra of individual SWNTs, giving rise to such unusual behavior of the G'-band feature as the presence of two peaks, observed for both semiconducting [12] and metallic [13] SWNTs. The appearance of two peaks in the G'-band Raman feature indicates that both the incident and scattered light are resonant with two different VHSs in the SWNT DOS. Shown in Figs. 1(b) and 1(c) are two SWNTs, semiconducting (17,6) and metallic (27,0), each having two VHSs within the 0.1 eV resonant window [14] of $E_{\text{laser}} = 2.41$ eV and $E_{\text{laser}} - E_{G'} = 2.08$ eV, $E_{44}^{\text{S}} = 2.36$ eV and $E_{33}^{\text{S}} = 2.08$ eV for (17,6), and $E_{22}^{\text{M}u} = 2.46$ eV and $E_{22}^{\text{M}l} = 2.15$ eV for (27,0), where the l and u indices denote the lower and upper energy components of E_{22}^{M}, and the splitting in E_{22}^{M} is due to the electronic trigonal warping effect [11]. For the (17,6) semiconducting SWNT [see Fig. 1(b)], $\mathbf{k}_3$ and $\mathbf{k}_4$ have different magnitudes, $k_4 - k_3 \cong K_1/3 = 2/(3d_t)$, which results in $q_4 - q_3 \cong 4/(3d_t)$ because of the relation $\mathbf{q}_i = -2\mathbf{k}_i$, and thus the G'-band splitting $\omega_{\text{ph}}(q_4) - \omega_{\text{ph}}(q_3)$ arises from the phonon dispersion $\omega_{\text{ph}}(q)$. In contrast, $\mathbf{k}_2^l$ and $\mathbf{k}_2^u$ for the (27,0) metallic SWNT [see Fig. 1(c)] have the same magnitude $k_2^l = k_2^u = 2K_1 = 4/d_t$ but opposite directions KM and $K\Gamma$. Thus, $\mathbf{q}_2^l$ and $\mathbf{q}_2^u$ also have the same magnitude and opposite directions, so that, for metallic SWNTs, the G'-band splitting arises from the anisotropy in $\omega_{\text{ph}}(\mathbf{q})$. Strictly speaking, the relation $\mathbf{k}_i^l = -\mathbf{k}_i^u$ holds only for zigzag metallic SWNTs while, for metallic SWNTs of other chiralities, it becomes approximate because of the electronic trigonal warping effect [11].

Details of the experimental setup and (n, m) assignments are discussed elsewhere [10]. To obtain the graphene phonon frequency ω_{ph} from the Raman shift of the SWNT G'-band $\omega_{G'}$, the latter is upshifted by 35.4 $(\text{cm}^{-1}\,\text{nm})/d_t$ to account for the force-constant softening due to the SWNT curvature [15]. The resulting $\omega_{G'}$ is divided by two because of the two equivalent phonons involved in the G'-band process. We have selected 11 SWNTs which best satisfy the preresonant condition $E_{\text{laser}} < E_{ii}$ (four resonant with E_{22}^{M}, three with E_{33}^{S}, and four with E_{44}^{S}, and the Ar^+ laser lines 2.41 and 2.54 eV were used). For the preresonant condition $E_{\text{laser}} < E_{ii}$, the only electronic state affecting the Raman spectra of SWNTs is the wave vector k_i, while in the opposite case ($E_{\text{laser}} > E_{ii}$), there is instead a group of resonant k states near the wave vector k_i along the cutting line, which results in the broadening of the DR Raman features. The phonon wave vectors for each SWNT were obtained using the DR condition $\mathbf{q}_i = -2\mathbf{k}_i$, where the electronic wave vectors $\mathbf{k}_i$ for the VHSs E_{ii} that are resonant with E_{laser} have been calculated using the tentative (n, m) assignments [10] in the nearest-neighbor tight-binding model [4] with the transfer integral energy $\gamma_0 = 2.89$ eV fitted for isolated SWNTs [10]. The 11 points $\omega_{\text{ph}}(\mathbf{q}_i)$ for the G'-band phonon mode around the K point (along with previously reported measurements on HOPG, graphite whiskers, and SWNT bundles for the other phonon modes) are fitted to the four-neighbor force-constant model [4], and the resulting force-constant parameters are summarized in Table I. The fitting procedure is described elsewhere [5]. The modification of the phonon dispersion relations from the previously fitted ones [2,5] is minor over the whole 2D BZ of graphite, but the amount of anisotropy around the K point differs substantially. The fit of the phonon dispersion for the G'-band phonon mode in the vicinity of the K point in the 2D BZ is plotted in Fig. 2(a) along with the 66 experimental q points (the 11 points expanded around the K point into six equivalent ΓKM sectors). The corresponding phonon equifrequency contours shown in Fig. 2(b) by solid lines demonstrate the trigonal warping effect in the $\omega_{\text{ph}}(\mathbf{q})$ as a distortion from the circular shape of the contours. For comparison, two electronic equienergy contours

TABLE I. Four-neighbor force constant parameters [2] in units of 10^4 dyn/cm. Subscripts r, ti, and to denote radial, transverse in-plane, and transverse out-of-plane components, respectively.

$\phi_r^{(1)} = 41.32$	$\phi_r^{(2)} = 1.22$	$\phi_r^{(3)} = -3.03$	$\phi_r^{(4)} = 3.80$
$\phi_{ti}^{(1)} = 23.65$	$\phi_{ti}^{(2)} = 3.98$	$\phi_{ti}^{(3)} = -11.50$	$\phi_{ti}^{(4)} = 0.93$
$\phi_{to}^{(1)} = 9.28$	$\phi_{to}^{(2)} = -0.08$	$\phi_{to}^{(3)} = -0.06$	$\phi_{to}^{(4)} = -0.62$

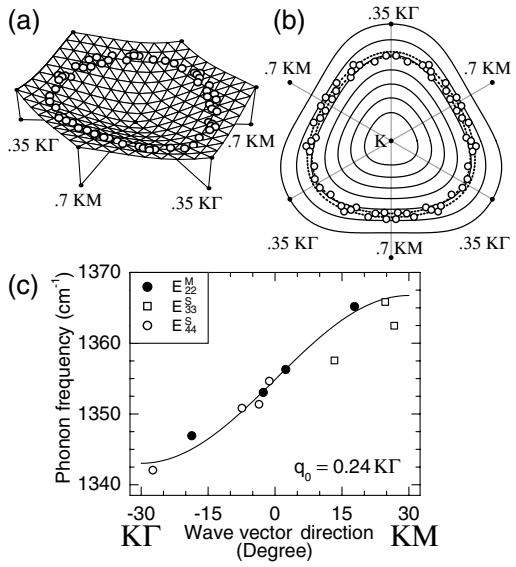

FIG. 2. (a) Phonon dispersion relations $\omega_{\text{ph}}(\mathbf{q})$ around the K point of the 2D BZ of graphite fitted to the experimental points $\omega_{\text{ph}}(\mathbf{q}_i)$ shown by dots. (b) Phonon equifrequency contours (solid lines), the experimental q points (dots), and corresponding electronic equienergy contours (dotted lines). (c) Dependence of $\omega_{\text{ph}}(\mathbf{q})$ on the q-vector direction for a given q magnitude $q_0 = 0.24K\Gamma$. The frequency difference for two different q-vector directions KM and $K\Gamma$ is $\Delta\omega_{\text{ph}} = 24\ \text{cm}^{-1}$.

corresponding to the laser energies 2.41 and 2.54 eV are plotted on the phonon wave vector surface of Fig. 2(b) by dotted lines, where the transformation $\mathbf{q}_i = -2\mathbf{k}_i$ from the electronic wave vector $\mathbf{k}_i$ to the phonon wave vector $\mathbf{q}_i$ is used. One can see in Fig. 2(b) that the phonon equifrequency contours and the electronic equienergy contours have different shapes, yet both are trigonally distorted, as discussed below. The experimental q points shown in Fig. 2(b) by dots are distributed along the electronic equienergy contours and not along the phonon equifrequency contours, reflecting the fact that RRS is resonant with respect to the electronic energy and not to the phonon frequency.

To visualize the phonon trigonal warping effect, we plot the frequency $\omega_{\mathrm{ph}}(\mathbf{q})$ as a function of the direction of the wave vector $\mathbf{q}$ for a given *magnitude* $|\mathbf{q}| = \overline{q}$. Since the 11 experimentally measured phonon frequencies $\omega_{\mathrm{ph}}(\mathbf{q}_i)$ correspond to different q-vector magnitudes $|\mathbf{q}_i| = q_i$ [see Fig. 2(b)], an interpolation scheme must be used to convert the frequencies to correspond to $\omega_{\mathrm{ph}}(\overline{q})$. Because the Raman-active phonon mode near the K point in the 2D BZ is linearly dispersive [16], and because the electronic dispersion is linear in k around the K point [4], we can approximate the phonon frequency shift by $\omega_{\mathrm{ph}}(q_i) - \omega_{\mathrm{ph}}(\overline{q}) = 53\ (\mathrm{cm}^{-1}/\mathrm{eV})(\sqrt{3}/2) \times \gamma_0 a(q_i - \overline{q})$, where $\overline{q} = q_0 = 0.24K\Gamma$, as discussed above. The resulting dependence of the phonon frequencies $\omega_{\mathrm{ph}}(\mathbf{q}_i)$ on the direction of the wave vectors $\mathbf{q}_i$ is shown in Fig. 2(c) by individual points for the 11 SWNTs, and the force-constant fit is shown by the solid curve. The fit gives a difference in the phonon frequencies $\Delta\omega_{\mathrm{ph}} = 24\ \mathrm{cm}^{-1}$ between the directions KM and $K\Gamma$. This value shows good agreement between the smallest linewidths of the D-band feature observed for graphite [17] ($\Gamma_{2\mathrm{D}} \sim 30\ \mathrm{cm}^{-1}$) and for SWNTs [18] ($\Gamma_{1\mathrm{D}} \sim 7\ \mathrm{cm}^{-1}$) with the laser line 2.41 eV, namely, $\Gamma_{2\mathrm{D}} \sim \Gamma_{1\mathrm{D}} + \Delta\omega_{\mathrm{ph}}$.

The phonon trigonal warping effect can be characterized quantitatively by the ratio of $\Delta\omega_{\mathrm{ph}} = 24\ \mathrm{cm}^{-1}$ to the phonon frequency change from the K point to the q_0 state. The latter can be estimated from the force-constant model [4], $\omega_{\mathrm{ph}}(q_0) - \omega_{\mathrm{ph}}(K) = 89\ \mathrm{cm}^{-1}$, so that the ratio is equal to $\Delta\omega_{\mathrm{ph}}/[\omega_{\mathrm{ph}}(q_0) - \omega_{\mathrm{ph}}(K)] = 27\%$. Similarly, the electronic trigonal warping effect can be characterized by the ratio $\Delta E_{ii}/E_{ii} = 17\%$, where $\Delta E_{ii} = 0.41$ eV is the maximum VHS transition energy splitting for a zigzag metallic SWNT at $E_{ii} = 2.41$ eV. The trigonal warping effect is thus larger for phonons than for electrons (27% vs 17%), in part, because it is probed at a different distance from the K point due to the DR condition $\mathbf{q}_i = -2\mathbf{k}_i$.

The phonon trigonal warping effect is revealed as a two-peak structure of the G'-band Raman feature observed for metallic SWNTs [13]. A similar two-peak structure of the G'-band for selected semiconducting SWNTs [12] is known to be related to the G'-band dispersion [16] with laser energy of $106\ \mathrm{cm}^{-1}/\mathrm{eV}$. By analogy with semiconducting SWNTs, the effective dispersion for metallic SWNTs is defined as a ratio of the G'-band splitting $2\Delta\omega_{\mathrm{ph}}$ to the transition energy splitting ΔE_{ii}^{M}, where the factor of 2 reflects the fact that two phonons are involved in the G'-band process. From our measurements of the phonon trigonal warping effect, the effective dispersion can be estimated by $2\Delta\omega_{\mathrm{ph}}/\Delta E_{ii} = 2 \times 24\ \mathrm{cm}^{-1}/0.41\ \mathrm{eV} = 117\ \mathrm{cm}^{-1}/\mathrm{eV}$. Direct measurement [13] of the effective dispersion for metallic SWNTs gives $108\ \mathrm{cm}^{-1}/\mathrm{eV}$, yielding good agreement with our phonon trigonal warping effect estimate.

In summary, the wave vector selective nature of the DR Raman process combined with quantum confinement of the wave vectors in low-dimensional systems allows us to measure directly trigonal warping-type effects in the phonon dispersion relations of graphite. Following the procedure given above, valuable information on the anisotropy of the 2D graphite phonon dispersion relations can be obtained, refining prior results of inelastic neutron scattering and RRS on graphitic materials.

The MIT authors acknowledge support under NSF Grants No. DMR 01-16042 and No. INT 00-00408. R. S. and A. G. acknowledge a Grant-in-Aid (No. 13440091) from the Ministry of Education, Japan. A. J. and A. G. S. F. acknowledge support from the Brazilian agency CNPq under Profix and DCR contracts, respectively.

[1] R. Saito *et al.*, Phys. Rev. Lett. **88**, 027401 (2002).
[2] R. A. Jishi *et al.*, Chem. Phys. Lett. **209**, 77 (1993).
[3] C. Thomsen and S. Reich, Phys. Rev. Lett. **85**, 5214 (2000).
[4] R. Saito, G. Dresselhaus, and M. S. Dresselhaus, *Physical Properties of Carbon Nanotubes* (Imperial College Press, London, 1998).
[5] A. Grüneis *et al.*, Phys. Rev. B **65**, 155405 (2002).
[6] R. Saito *et al.*, Jpn. J. Appl. Phys. **41**, 4878 (2002).
[7] A. Grüneis *et al.* (to be published).
[8] A. Jorio *et al.* (to be published).
[9] H. Ajiki and T. Ando, J. Phys. Soc. Jpn. **62**, 2470 (1993).
[10] A. Jorio *et al.*, Phys. Rev. Lett. **86**, 1118 (2001).
[11] R. Saito, G. Dresselhaus, and M. S. Dresselhaus, Phys. Rev. B **61**, 2981 (2000).
[12] A. G. Souza Filho *et al.*, Phys. Rev. B **65**, 085417 (2002).
[13] A. G. Souza Filho *et al.*, Chem. Phys. Lett. **354**, 62 (2002).
[14] A. Jorio *et al.*, Phys. Rev. B **63**, 245416 (2001).
[15] A. G. Souza Filho *et al.*, Phys. Rev. B (to be published).
[16] M. A. Pimenta *et al.*, Braz. J. Phys. **30**, 423 (2000).
[17] H. Wilhelm *et al.*, J. Appl. Phys. **84**, 6552 (1998).
[18] A. Jorio *et al.*, Phys. Rev. B **66**, 115411 (2002).